buildings

MDPI

Article

Mechanical Performance and Water Stability of Gobi Soil Reinforced with Polypropylene Fibers for Photovoltaic Power Station Foundations

Xiaoyang Liu [1,*], Jiayu Wang [1], Ziyang Zhang [1], Jin Wu [1] and Di Wu [2]

[1] College Civil Engineering & Architecture, Xinjiang University, Urumqi 830047, China; wangjiayu@stu.xju.edu.cn (J.W.); wujin@xju.edu.cn (J.W.)
[2] College of Construction Engineering, Jilin University, Changchun 130021, China
* Correspondence: liuxiaoyang24@xju.edu.cn

Abstract

The poor engineering properties of Gobi soil, such as low strength and poor water stability, pose challenges for foundations in arid regions, especially large photovoltaic plants. This study examines the effect of polypropylene (PP) fiber reinforcement on Gobi soil from Dabancheng, Xinjiang. Laboratory tests including unconfined compressive strength, direct shear (orthogonal experimental design), slake durability, and scanning electron microscopy were performed to investigate the influences of fiber length (6, 9, 12 mm), fiber content (0.3–1.1% by dry soil mass), and water content (4–12.5%). Results indicate that PP fibers change the failure mode from brittle to ductile. The optimal combination (9 mm fiber length, 0.7% content, and Proctor optimum water content of 10.5% corresponding to maximum dry density) improves cohesion by 122% (reinforcement coefficient K = 2.22). Moreover, fibers alter the disintegration behavior from complete to stable partial disintegration; the 12 h disintegration ratio decreases from 100% to 13% under optimal conditions. Microstructural analysis shows that an appropriate fiber content creates a uniform three-dimensional reinforcing network, enhancing mechanical interlocking and fiber bridging, whereas excessive fiber leads to agglomeration and increased pore connectivity, degrading overall performance. This study provides a low-carbon, sustainable soil stabilization method and practical design parameters for Gobi desert infrastructure.

Keywords: Gobi soil; polypropylene fiber reinforcement; water stability; mechanical performance; low-carbon

Check for updates

Academic Editor: Eugeniusz Koda

Received: 16 May 2026
Revised: 14 June 2026
Accepted: 20 June 2026
Published: 23 June 2026

Copyright: © 2026 by the authors. Licensee MDPI, Basel, Switzerland. This article is an open access article distributed under the terms and conditions of the Creative Commons Attribution (CC BY) license.

1. Introduction

The arid and semi-arid regions of northwest China host approximately 661,200 km^2 of Gobi desert, accounting for roughly 6.9% of the country's total land area. This region not only functions as a strategic corridor linking Central Asia and Europe but also boasts abundant wind and solar energy resources and vast available land, making it an ideal site for the construction of large-scale wind and photovoltaic (PV) power bases. The development of clean energy in this region helps optimize China's national energy layout and convert its resource endowments into economic momentum, which is of great significance for advancing coordinated regional development and achieving the national "Dual Carbon" strategic goals [1–3]. Gobi areas across Xinjiang, Gansu, and Inner Mongolia have been designated as national-level PV energy bases [4,5]. By 2025, China has set a target of 3.3 trillion kWh of annual renewable energy generation, with its total installed wind

and solar capacity expected to double from current levels [6,7]. Xinjiang alone accounts for approximately 40% of China's total wind energy resources and features top-tier solar energy resources [8]. In 2024, investment in traditional infrastructure in Xinjiang exceeded 100 billion yuan, while investment in new energy infrastructure—including wind power, PV, and power grid projects—grew at an even faster rate, with multiple projects each worth tens of billions of yuan currently under construction [9]. As a result, large volumes of Gobi soil will be utilized as construction material for subgrades, equipment platforms, and foundation works. Accordingly, the systematic evaluation and improvement of the engineering properties of Gobi soil is critical for ensuring the safety, durability, and lifecycle cost-effectiveness of infrastructure projects [10].

However, Gobi soil presents significant engineering challenges when utilized as a foundation construction material. It is a poorly graded coarse-grained soil with a fines content (especially clay fraction) typically below 5%, which gives rise to low inherent cohesion, a loose granular structure, and poor structural stability [11–14]. Wind turbine and PV facility foundations impose stringent performance requirements on subgrade materials, which cannot be satisfied by untreated Gobi soil in its natural state [15,16]. Harsh cyclic environmental conditions in Xinjiang—including extreme diurnal temperature fluctuations, repeated dry–wet alternations, and freeze–thaw cycles—further deteriorate its engineering properties [17,18]. Under long-term operational loads and cyclic environmental effects, foundations built on untreated Gobi soil are susceptible to differential settlement, cracking, ground heave, subgrade instability, and slope erosion [19–22]. Field engineering data show that the defect rate of infrastructure foundations in Gobi regions is 30–40% higher than that in cohesive soil regions, and the accompanying safety hazards and elevated maintenance costs pose a tangible threat to the advancement of China's new energy development strategy [23–26]. Conventional ground improvement methods exhibit notable limitations in Gobi desert engineering applications: the soil replacement method entails long-distance material transportation, high construction costs, and substantial energy consumption, while also causing irreversible damage to the fragile Gobi ecosystem [27–32]. Cement and lime stabilization can effectively enhance soil strength, but both processes are highly energy-intensive and carbon-intensive, as the global cement industry alone accounts for approximately 7% of total anthropogenic CO_2 emissions, with roughly 0.9 tonnes of CO_2 generated per tonne of cement produced [33,34], rendering such chemical stabilization approaches misaligned with China's "Dual Carbon" strategic goals. Furthermore, soils stabilized by these chemical binders exhibit inherently brittle failure characteristics and are prone to cracking under cyclic temperature and moisture variations [31,35–38]. Accordingly, there is an urgent demand for an efficient, cost-effective, low-carbon, and eco-friendly soil stabilization method specifically tailored to the unique engineering properties of Gobi soil.

Fiber reinforcement represents a promising alternative soil stabilization technique. Randomly dispersed fibers within the soil matrix form a three-dimensional reinforcing network that restricts soil particle displacement, transfers applied loads, and inhibits crack initiation and propagation [39–43], thereby improving the structural integrity, tensile strength, and erosion resistance of the soil [44–48]. Common fiber types can be categorized into natural fibers (e.g., rice husk fiber, straw fiber, basalt fiber) [46–52] and synthetic fibers (e.g., polypropylene, polyester, and glass fiber) [53–56]. Among synthetic fibers, polypropylene (PP) fiber is especially suitable for Gobi soil stabilization, owing to its low embodied energy in production, excellent chemical stability, corrosion resistance, high tensile strength, low unit weight, cost-effectiveness, and recyclability. Its engineering performance is more durable and stable than that of natural fibers, while its carbon footprint is significantly lower than that of most other synthetic fibers [57–59]. While the reinforcement effect of PP fiber has been extensively investigated in sandy and clayey soils, systematic studies on its

application to the unique Gobi soil in northwest China remain scarce [60–63]. Gobi soil differs fundamentally from fine-grained soils in terms of fiber–soil interaction mechanisms: due to its distinct particle characteristics and interfacial properties, the interaction between fibers and Gobi soil is dominated by mechanical interlocking and interparticle friction rather than surface adhesion [64–66]. Furthermore, existing studies have predominantly focused on improvements in macroscopic strength properties, while failing to systematically investigate how fiber parameters (i.e., length and content) interact with key soil state variables (e.g., water content) to influence the stress–strain behavior, water stability, and microstructural evolution of reinforced Gobi soil.

To address these research gaps and promote the application of PP fiber reinforcement technology for foundation engineering in Gobi regions (particularly for photovoltaic power stations), this study presents a comprehensive investigation of PP fiber-reinforced Gobi soil sampled from Dabancheng, Xinjiang. A series of laboratory tests was employed, including unconfined compressive strength (UCS) tests, direct shear tests designed with an orthogonal experimental scheme (investigating three variables: fiber length of 6, 9, and 12 mm, fiber content of 0.3–1.1% by dry soil mass, and water content of 4–12.5%), slake durability tests, and scanning electron microscopy (SEM) observations. The specific research objectives are as follows: (1) to quantify the influences of fiber length and dosage on the compressive strength, stress–strain behavior, and failure mode of reinforced Gobi soil; (2) to evaluate the combined effects of fiber parameters and water content on shear strength indices (i.e., cohesion and internal friction angle), conduct multidimensional statistical analyses (including range analysis, analysis of variance (ANOVA), and Taguchi signal-to-noise (S/N) ratio analysis), and develop empirical prediction models; (3) to assess the improvement in water stability, with a focus on the transition of soil disintegration behavior from complete disintegration to stable partial disintegration; (4) to reveal the underlying microstructural reinforcement mechanisms, involving the formation of a three-dimensional reinforcing network, fiber bridging effects, and crack inhibition. Based on comprehensive experimental analysis, the optimal fiber parameters are identified as a 9 mm fiber length and 0.7% fiber content. This research proposes a low-carbon, sustainable approach for Gobi soil stabilization, and provides practical design parameters to support the reliable construction of infrastructure foundations in Gobi desert environments.

2. Materials

2.1. Gobi Soil

Gobi soil specimens used in this study were sampled from a wind farm site in Dabancheng District, Urumqi City, Xinjiang Uygur Autonomous Region, China. Prior to testing, the raw soil samples were air-dried, gently crushed, and sieved through a 5 mm sieve to eliminate oversized particles. Figure 1 illustrates the sampling location and particle size distribution curve of the test soil, and its basic physical and engineering properties are summarized in Table 1. Particle size analysis indicates that the soil is dominated by sand-sized particles, accounting for 84.3% of the total mass, followed by 6.7% fine gravel and only 9.0% fines (particles smaller than 0.075 mm), which confirms its typical coarse-grained nature. The optimum water content and maximum dry density of the soil, determined via standard Proctor compaction tests, were 10.5% and 2.07 $g \cdot cm^{-3}$, respectively. The primary mineral composition of the Gobi soil was identified through X-ray diffraction (XRD) analysis (Equipment: D8 ADVANCE X-ray diffractometer (Bruker AXS GmbH, Karlsruhe, Germany)), and its major chemical components were characterized via X-ray fluorescence (XRF) spectroscopy (Equipment: ZSX Primus X-ray fluorescence spectrometer (Rigaku Corporation, Tokyo, Japan)); the corresponding results are presented in Figure 2.

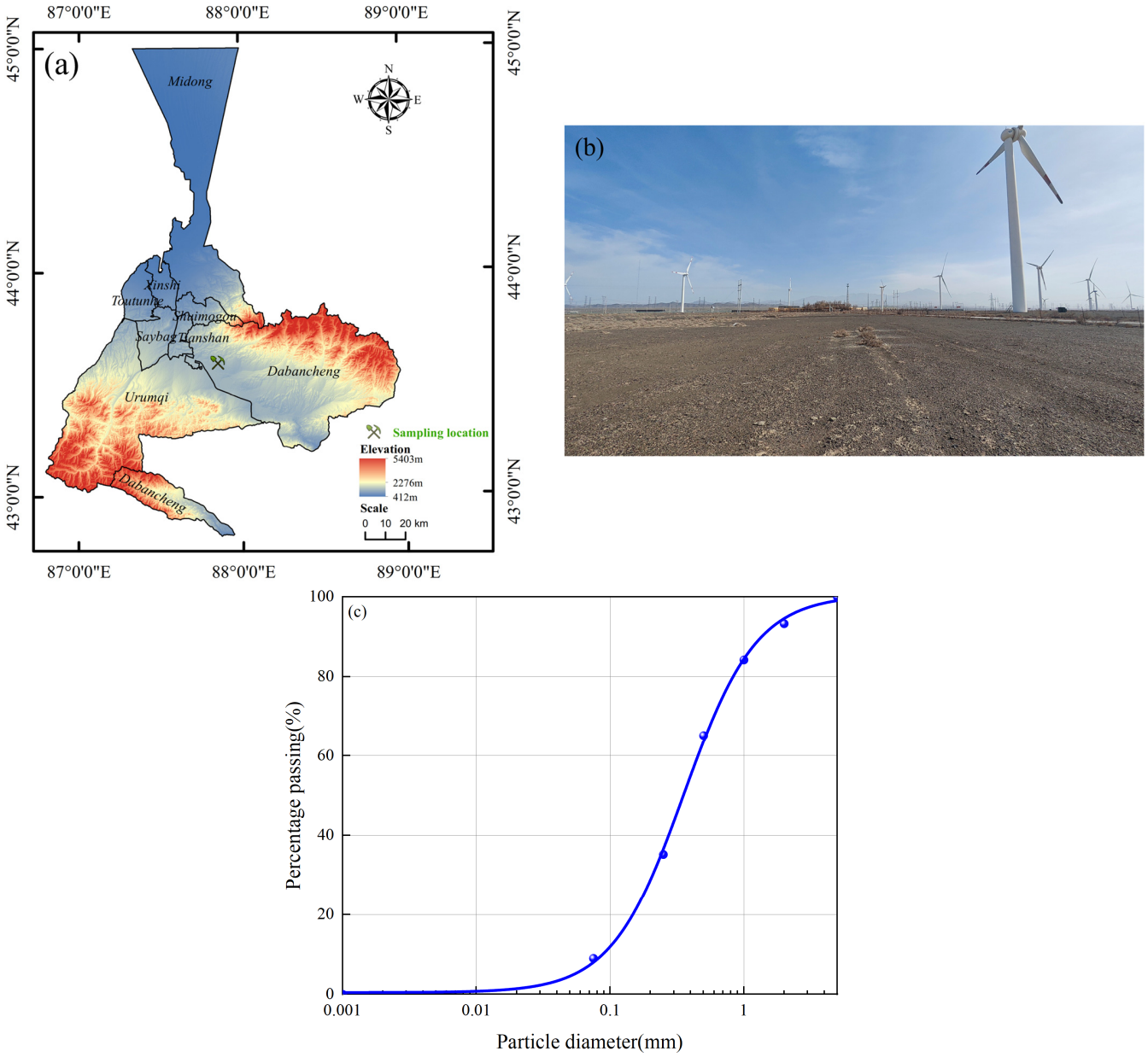


Figure 1. Geographical location of sampling: (**a**) topographic map of the sampling site; (**b**) Gobi soil; (**c**) Grain size distribution curve of Gobi soil [67].

Table 1. Engineering properties of Gobi soil.

Properties	Result
Type	Gobi soil (GS)
Specific gravity (-)	2.70
Fine gravel, 2 mm–5 mm (%)	6.7
Sand grain, 0.075 mm~2 mm (%)	84.3
Fine grain, <0.075 mm (%)	9.0
Optimum water contents (%)	10.5
Maximum dry density (g/cm^3)	2.07
Liquid limit (Particle size < 0.5 mm) (%)	16.3
Plastic limit (Particle size < 0.5 mm) (%)	12.5

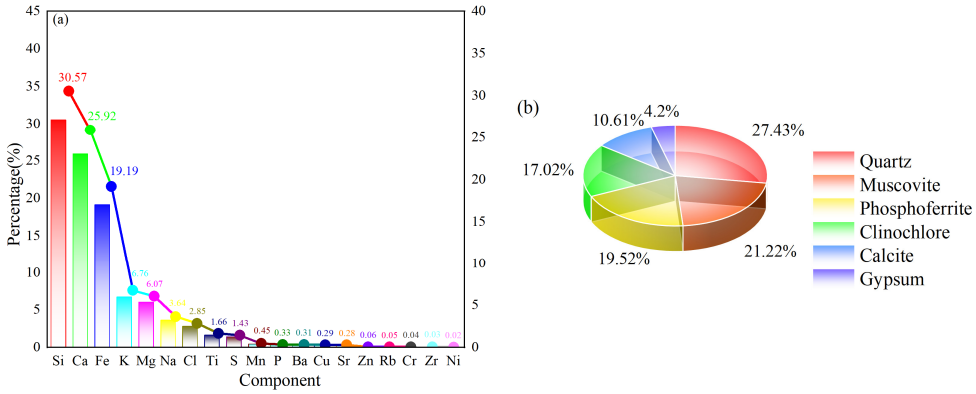


Figure 2. Results of XRD and XRF: (**a**) relative content of primary chemical components; (**b**) relative content of primary minerals.

2.2. Polypropylene Fiber

Polypropylene (PP) fibers, manufactured by Shandong Binzhou Xianghe Chemical Fiber Products Co., Ltd. (Binzhou, China), were selected as the reinforcing material in this study. Three fiber lengths—6 mm, 9 mm, and 12 mm—were adopted to systematically investigate the influence of fiber length on reinforcement performance. These PP fibers are fabricated from isotactic polypropylene through propylene polymerization followed by melt spinning, a manufacturing process characterized by environmental friendliness and a low carbon footprint. The basic physical properties of the fibers are summarized in Table 2.

Table 2. Physical properties of polypropylene fiber.

Properties	Result
Type	Polypropylene (PP) fiber
Fracture Strength (MPa)	576
Initial modulus (GPa)	4.9
Equivalent diameter (μm)	36.13
Length (mm)	6, 9, 12

3. Sample Preparation and Tests

3.1. Sample Preparation

First, the raw Gobi soil and polypropylene (PP) fibers were pre-dried to achieve a consistent initial moisture state. Next, PP fibers of the selected lengths (6 mm, 9 mm, and 12 mm) were added to the dried Gobi soil in batches at predetermined mass dosages (0.3%, 0.5%, 0.7%, 0.9%, and 1.1% by dry soil mass), and the blend was thoroughly dry-mixed for no less than 3 min to mitigate fiber agglomeration. Distilled water was then uniformly sprayed onto the dry mixture to reach the target water contents (4%, 6%, 8%, 10.5%, and 12.5%), followed by 2 min of wet mixing to ensure random, uniform fiber dispersion within the soil matrix. The resulting homogeneous mixture is hereafter designated as polypropylene fiber-reinforced Gobi soil, abbreviated as PP-GS. The moist soil mixture was sealed in airtight plastic bags and stored for 24 h to enable uniform moisture redistribution and equilibration. Finally, cylindrical specimens of varying dimensions were prepared via static compaction to attain 95% of the maximum dry density. For the 20 mm-high direct shear specimens, three-layer compaction was adopted, with the surface of each underlying layer scarified before the next layer was added; this procedure avoids preferential horizontal fiber alignment and preserves the three-dimensional random distribution of fibers in the specimens. A schematic of the overall experimental procedure employed in this study is presented in Figure 3.

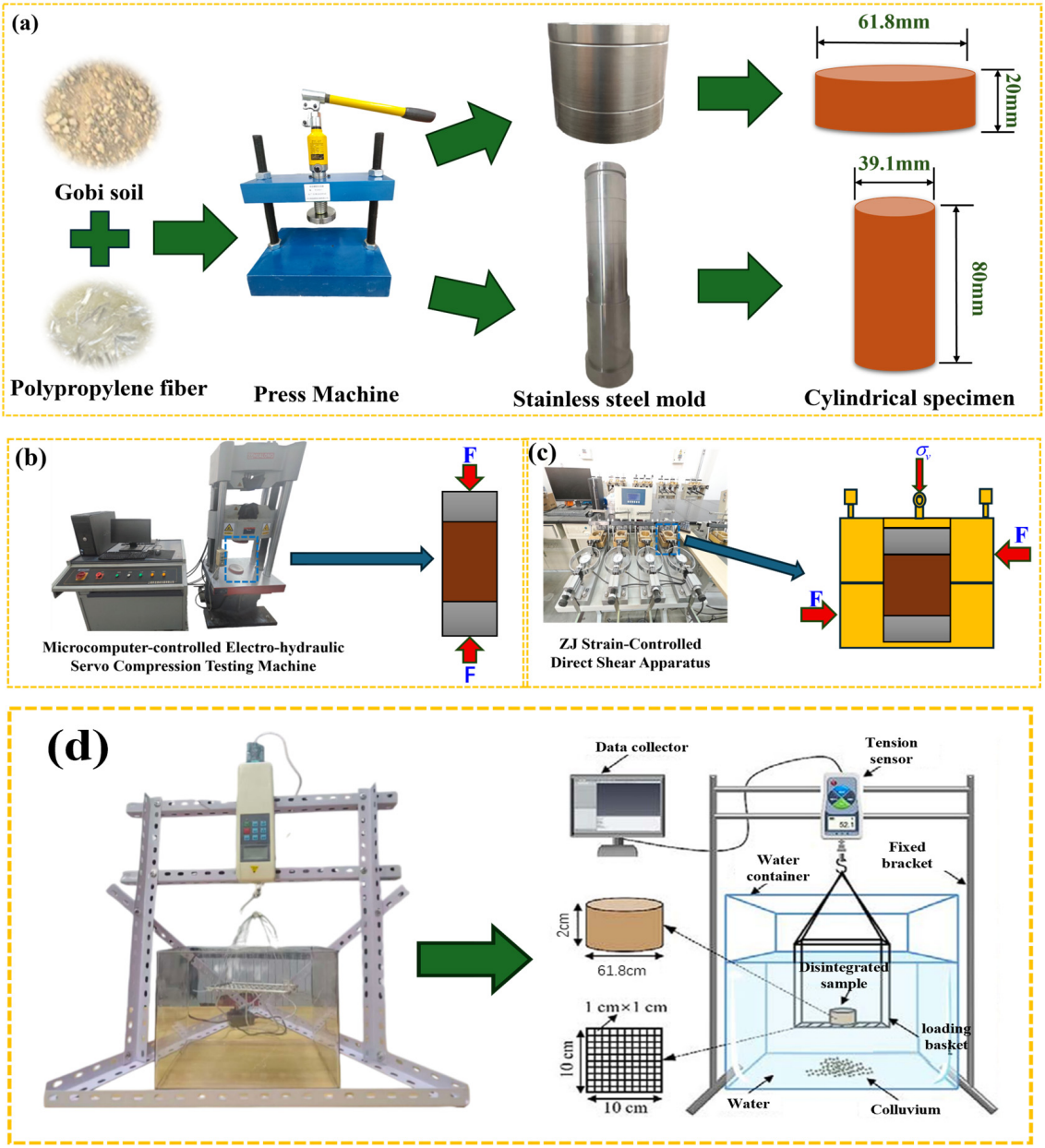


Figure 3. Procedures and instruments used for tests: (**a**) compacted specimen; (**b**) unconfined compressive test; (**c**) direct shear test; (**d**) water stability test.

3.2. Unconfined Compressive Tests

Unconfined compressive strength (UCS) tests (Equipment: WDW-200 universal testing machine (Shanghai Hualong Testing Instrument Co., Ltd., Shanghai, China)) were performed to assess the influences of fiber content and fiber length on the compressive behavior of PP fiber-reinforced Gobi soil (PP-GS). All specimens were prepared at the optimum water content (w_{opt} = 10.5%), with fiber lengths of 0, 6, 9, and 12 mm and fiber contents of 0.0%, 0.3%, 0.5%, 0.7%, 0.9%, and 1.1% by dry soil mass. The detailed test scheme is presented in Table 3. Cylindrical specimens measuring 39.1 mm in diameter and 80 mm in height were adopted for the tests. In accordance with the Standard for Geotechnical Testing Methods (GB/T 50123–2019) [68], all tests were conducted at a constant axial loading rate of 2.4 mm·min^{-1}. Each test was terminated when the axial strain reached 16% of the specimen height; loading continued even after the axial load reached its peak value or stabilized, to fully capture the post-peak stress–strain response of the specimens.

Table 3. UCS test scheme.

Properties	Experiment Setting
Fiber length (mm)	0, 6, 9, 12
Fiber content (%)	0.0, 0.3, 0.5, 0.7, 0.9, 1.1
Water content (%)	10.5 (w_{opt})
Number of samples	$3 \times 5 + 1 = 16$
Parallel specimens per group	2

3.3. Direct Shear Tests

Direct shear tests (Equipment: ZJ strain-controlled automatic direct shear apparatus, manufactured by Nanjing Soil Instrument Factory Co., Ltd., Nanjing, China) were conducted to investigate the combined effects of fiber content, fiber length, and water content on the shear strength parameters of PP-GS. A standard $L_{25}(5^2 \times 3^1)$ mixed-level orthogonal experimental design was adopted: fiber content and water content were set to five levels to accurately delineate the optimal parameter range for the highly sensitive Gobi soil, while fiber length was set to three levels (6 mm, 9 mm, and 12 mm) to fully cover the effective length range for engineering applications and minimize redundant testing. All tests were performed on cylindrical specimens measuring 61.8 mm in diameter and 20 mm in height, under four normal stress levels of 50 kPa, 100 kPa, 200 kPa, and 400 kPa. In accordance with the Standard for Geotechnical Testing Methods (GB/T 50123–2019), a quick shear procedure was applied at a constant shear rate of 1.2 mm·min^{-1}, and each test was terminated when shear displacement reached 6 mm. For data analysis, range analysis was performed based on the mean value of test indices at each factor level to eliminate bias arising from unequal sample sizes; analysis of variance (ANOVA) was conducted using a general linear model (GLM) with Type III sum of squares, which accommodates unbalanced data structures and ensures the statistical robustness of conclusions regarding the effect of fiber length. The detailed experimental scheme is presented in Table 4.

Table 4. Direct Shear test scheme (Orthogonal Design).

Number	Fiber Length (mm)	Fiber Content (%)	Water Content (%)
1	6	0.3	4
2	6	0.5	8
3	6	0.7	12.5
4	6	0.9	6
5	6	1.1	10.5
6	9	0.3	12.5
7	9	0.5	6
8	9	0.7	10.5
9	9	0.9	4
10	9	1.1	8
11	12	0.3	10.5
12	12	0.5	4
13	12	0.7	8
14	12	0.9	12.5
15	12	1.1	6
16	6	0.3	8
17	6	0.5	12.5
18	6	0.7	6
19	6	0.9	10.5
20	6	1.1	4
21	9	0.3	6
22	9	0.5	10.5

Table 4. *Cont.*

Number	Fiber Length (mm)	Fiber Content (%)	Water Content (%)
23	9	0.7	4
24	9	0.9	8
25	9	1.1	12.5

3.4. Water Stability Tests

Upon water immersion, soil is prone to erosive disintegration driven by water softening and particle scouring. To replicate water-induced erosion behavior and systematically evaluate the influences of fiber content, fiber length, and initial water content on the water stability of fiber-reinforced Gobi soil, static immersion disintegration tests were conducted using a self-developed test apparatus, with the detailed specimen parameters summarized in Table 5. The apparatus is primarily composed of a water tank, a perforated metal grid plate, and a high-precision force sensor (Equipment: SH-10N digital force gauge (Wenzhou Weidu Electronics Co., Ltd., Wenzhou, China)) equipped with real-time data communication functionality. Cylindrical specimens were placed on the metal grid plate, which was suspended vertically from the force sensor. The continuous mass loss process of the specimens was recorded in real time by a connected computer, while the morphological evolution of the specimens throughout the disintegration process was documented by a digital camera (Figure 3). Each test was terminated either when the specimen underwent complete disintegration or after a continuous immersion period of 12 h.

Table 5. Water stability test scheme.

Number	Fiber Length (mm)	Fiber Content (%)	Water Content (%)
1	0	0	6
2	0	0	10.5
3	0	0	12.5
4	9	0.7	6
5	9	0.7	10.5
6	9	0.7	12.5
7	6	0.7	10.5
8	12	0.7	10.5

The disintegration ratio of the specimen was calculated according to the following equation:

$$C_t = \frac{m_0 - m_t}{m_0} \times 100\% \quad (1)$$

where C_t is the disintegration percentage of the sample (%); m_t is the mass of the sample at time t, and m_0 is the initial mass of the sample.

3.5. SEM Tests

Small cubic specimens measuring approximately 10 mm × 10 mm × 10 mm were carefully excised from the central portion of post-test UCS specimens, and subsequently prepared for microstructural characterization via scanning electron microscopy (SEM) to systematically analyze the micromorphological features and pore distribution patterns of fiber-reinforced Gobi soil. The secondary electron imaging mode was employed to characterize the interfacial contact state at the fiber–soil interface, the spatial distribution of fibers within the soil matrix, and the packing arrangement of soil particles. Detailed specimen parameters are summarized in Table 6.

Table 6. SEM test scheme.

Fiber Length (mm)	Fiber Content (%)	Water Content (%)
9	0 0.3 0.5 0.7 0.9 1.1	10.5

4. Results and Discussion

4.1. Unconfined Compressive Strength Characteristics

Figure 4 shows the stress–strain curves of PP-GS specimens with varying fiber lengths obtained from unconfined compressive strength (UCS) tests. For the unreinforced specimen (designated 0PP-GS, i.e., PP-GS with a fiber content of 0%), the initial portion of its stress–strain curve exhibits an approximately linear trend, corresponding to the elastic deformation stage of the soil. Upon reaching the peak stress, the soil strength drops abruptly, and the specimen undergoes typical brittle failure. With the incorporation of PP fibers, the initial segment of the curves no longer retains a linear profile; instead, it displays pronounced nonlinear characteristics. This behavior indicates that fiber inclusion modifies the internal structure of the soil matrix and induces a distinct compaction phase during the loading process. This mechanical response is in good agreement with the findings reported in previous relevant studies [48].

After reaching peak strength, fiber-reinforced PP-GS specimens retain considerable residual strength, with a markedly reduced rate of strength degradation. As illustrated in Figure 5, the unreinforced 0PP-GS specimen fails along a distinct through-going shear fracture plane, whereas fiber-reinforced specimens predominantly exhibit lateral bulging deformation, accompanied only by scattered surface microcracks. Taken together, the stress–strain response and observed failure patterns confirm that the unreinforced specimen displays typical brittle failure characteristics, while fiber-reinforced Gobi soil exhibits pronounced ductile failure behavior.

Figure 6 compares the unconfined compressive strength (UCS) of PP-GS specimens with varying fiber lengths and dosages. The test results demonstrate that UCS first increases and then decreases with increases in both fiber length and fiber content. This trend can be explained by the following mechanism: at appropriate dosages, fibers effectively suppress crack initiation and propagation during compressive loading, thereby enhancing the toughness and compressive strength of the soil matrix [48]. However, once the fiber content or length exceeds a critical threshold, excessive fibers tend to agglomerate within the soil matrix, forming localized weak zones and potential fracture planes that in turn reduce the overall soil strength [44,55]. This "critical fiber parameter" phenomenon has also been widely verified in studies on other types of fiber-reinforced soils [54,56]. Based on the experimental results, the optimal fiber content and length for PP-GS in this study are identified as 0.7% and 9 mm, respectively.

4.2. Direct Shear Strength Characteristics

4.2.1. Effect on Peak Shear Strength

Figure 7 presents the peak shear strength (τ_{max}) of fiber-reinforced Gobi soil under normal stresses (σ_n) ranging from 50 kPa to 400 kPa, covering five initial water contents (4%, 6%, 8%, 10.5%, and 12.5%, corresponding to Figure 7a–e) across fiber contents of 0.3–1.1% and fiber lengths of 6–12 mm. As expected, peak shear strength increases mono-

tonically with rising normal stress for all specimen groups. Although direct shear and UCS tests yield divergent results owing to differences in stress states and failure mechanisms, the optimal parameter combination (0.7% fiber content and 9 mm fiber length) consistently delivers superior mechanical performance across most test conditions. Under low-to-moderate water contents (Figure 7a–d), this combination achieves high peak shear strength under medium and high normal stresses; its shear performance is comparable to that of specimens with higher fiber contents (0.9–1.1%) or longer fibers (12 mm), while avoiding the detrimental effects of fiber agglomeration. Even under the high water content condition (12.5%), where interparticle interactions are weakened by excess pore water, the optimal combination still outperforms the low-fiber scheme (0.3% dosage with 6 mm length) and remains competitive with high-fiber configurations. Fiber contents above 0.9% or fiber lengths of 12 mm produce only marginal strength gains and exhibit strength saturation under high normal stresses, which can be attributed to the diminishing marginal returns of fiber reinforcement.

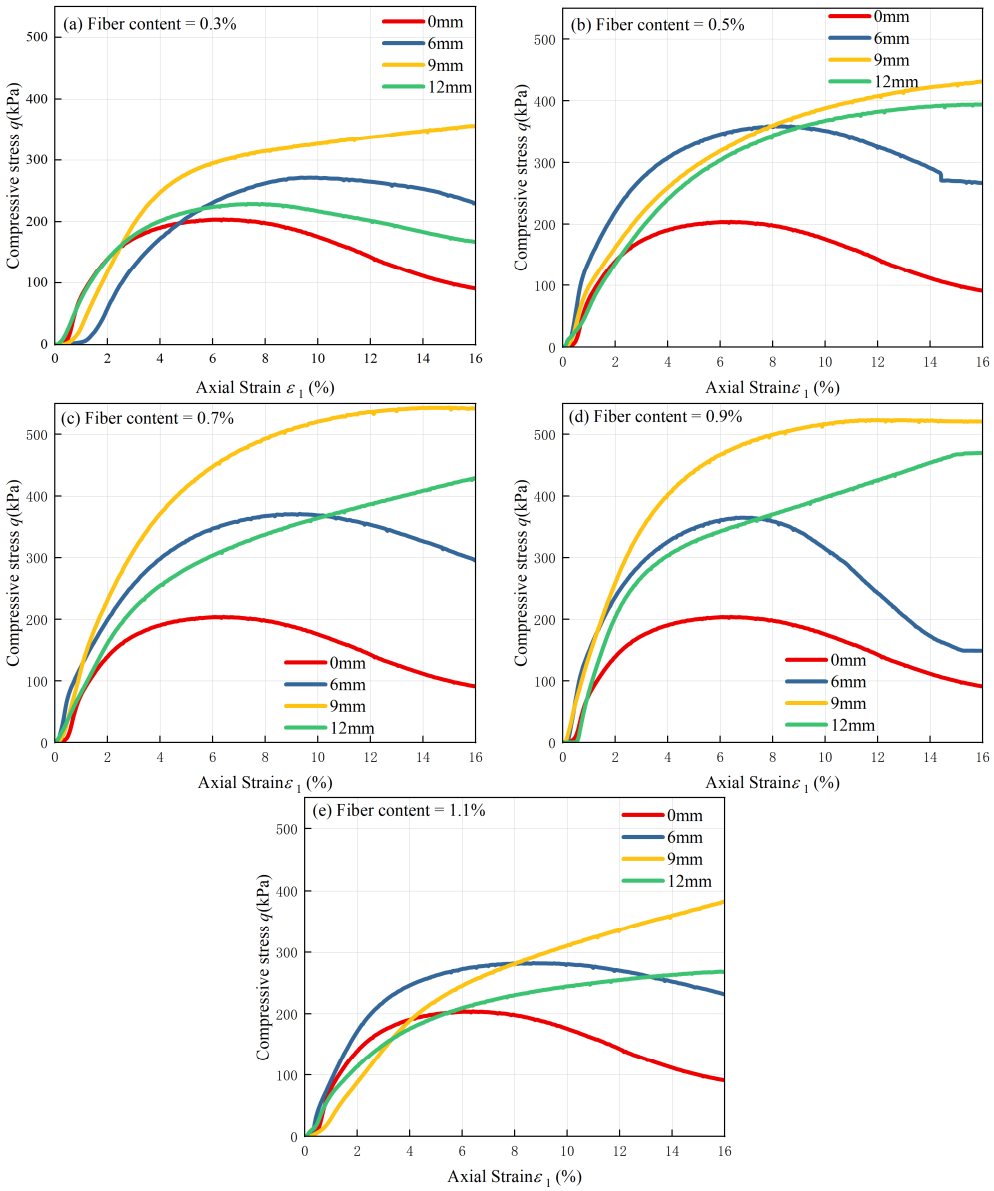


Figure 4. Unconfined compressive stress–strain curves of PP-GSs with different fiber lengths: (**a**) fiber content = 0.3%; (**b**) fiber content = 0.5%; (**c**) fiber content = 0.7%; (**d**) fiber content = 0.9%; (**e**) fiber content = 1.1%.

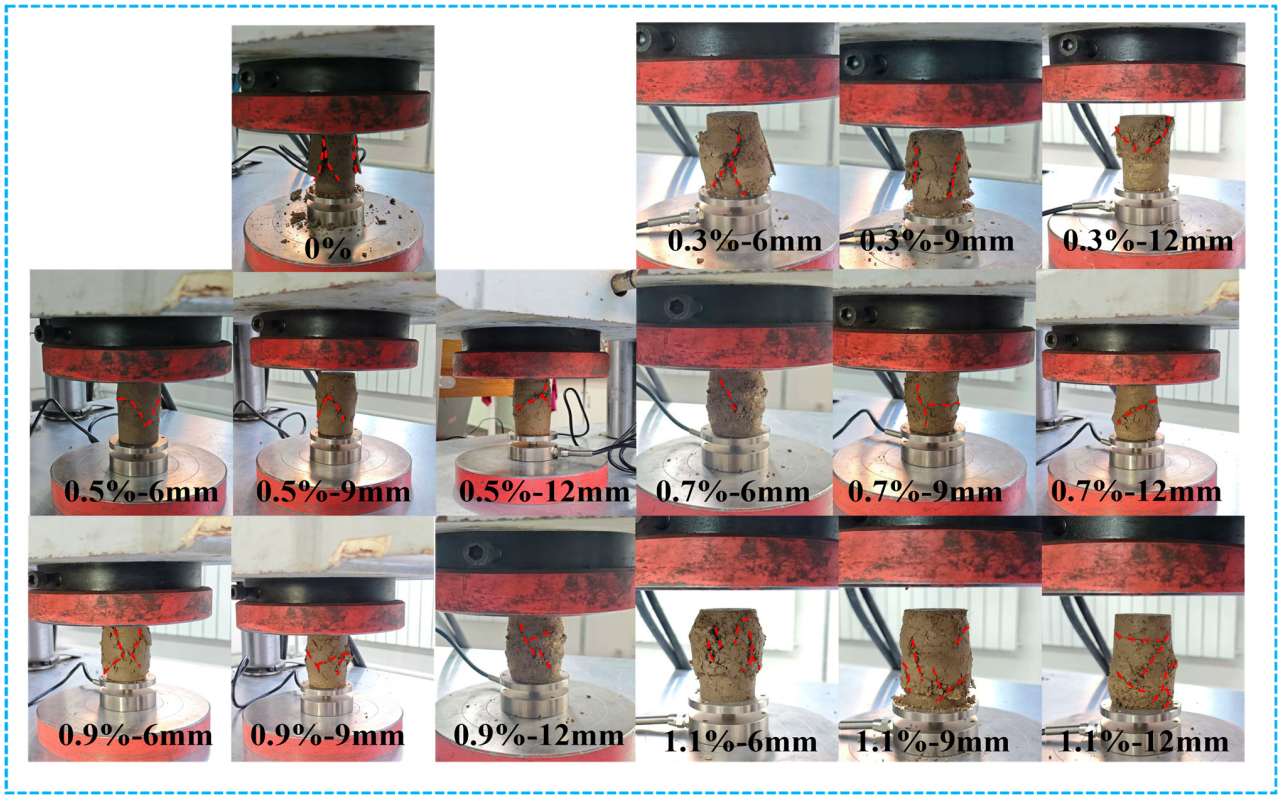


Figure 5. Failure modes of PP-GSs in unconfined compressive test.

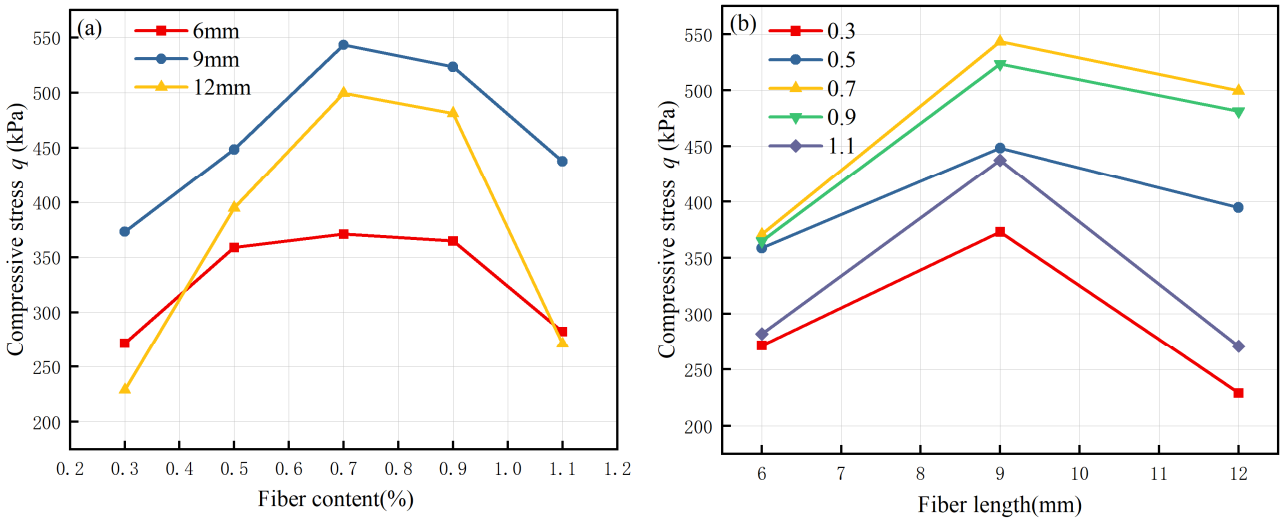


Figure 6. Unconfined compressive strength of PP-GSs with different fiber contents and fiber lengths: (**a**) fiber content; (**b**) fiber length.

4.2.2. Shear Strength Indices

Table 7 summarizes the shear strength parameters (cohesion c and internal friction angle φ) of fiber-reinforced Gobi soil. The corresponding baseline values for unreinforced soil at each water content are taken from our previous systematic study on the same batch of Gobi soil [67]; all specimens were prepared using identical procedures and tested with the same equipment following standardized protocols, ensuring the reliability of comparative analyses of relative reinforcement performance. Fiber reinforcement produces a far more pronounced improvement in soil cohesion than in the internal friction angle. To quantify this cohesion enhancement, a reinforcement coefficient K is introduced, defined as the ratio

of the cohesion of fiber-reinforced soil to that of the corresponding unreinforced soil under matching water content conditions:

$$K = C_r / C_0 \quad (2)$$

where K is the reinforcement coefficient and dimensionless, and C_r and C_0 are the cohesion after and before reinforcement, respectively. The corresponding calculated results are also listed in Table 7.

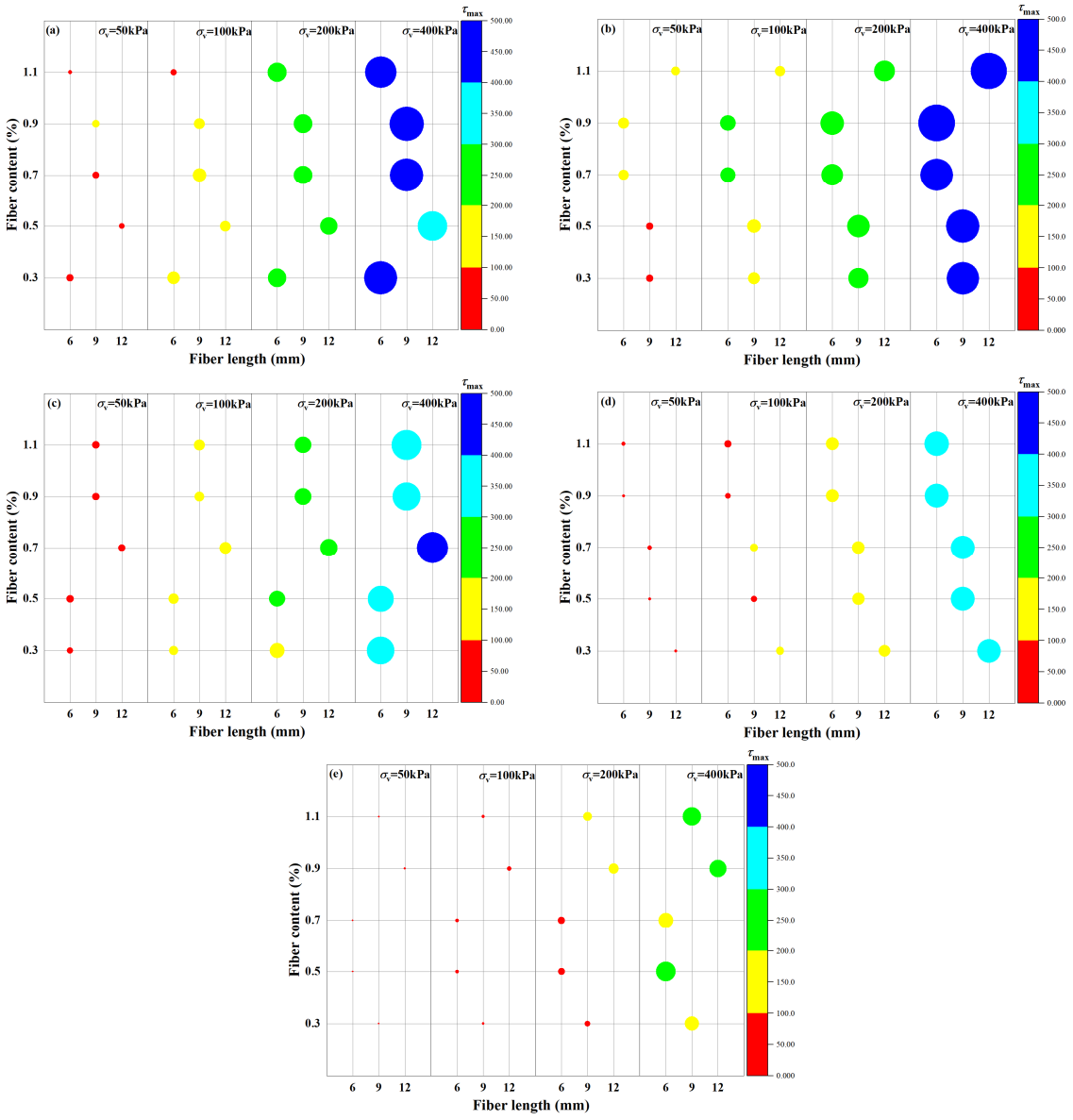


Figure 7. Peak shear strength of PP-GSs with different fiber lengths and fiber contents: (**a**) water content = 4%; (**b**) water content = 6%; (**c**) water content = 8%; (**d**) water content = 10.5%; (**e**) water content = 12.5%.

Based on 25 orthogonal direct shear tests with three variables—fiber length (FL), fiber content (FC), and initial water content (WC)—a systematic multi-dimensional statistical analysis, including mean response analysis, range analysis, frequency distribution analysis, analysis of variance (ANOVA), and Taguchi signal-to-noise (S/N) ratio analysis, was performed for cohesion c and internal friction angle φ. The corresponding results are presented in Figure 8 (cohesion) and Figure 9 (internal friction angle).

Table 7. Shear Strength Parameters and Reinforcement Coefficient of Fiber-Reinforced Soil.

Number	*c* (kPa)	*K*	*φ* (°)
1	66.64	1.07	41.99
2	53.22	1.10	36.21
3	10.39	1.56	24.34
4	86.83	1.14	44.70
5	21.18	1.03	36.37
6	10.15	1.52	22.23
7	95.27	1.25	40.40
8	45.77	2.22	32.44
9	78.88	1.27	41.48
10	57.26	1.19	39.45
11	21.74	1.05	34.65
12	67.54	1.08	37.80
13	59.84	1.24	40.70
14	8.81	1.32	28.86
15	76.50	1.00	43.55
16	49.54	1.03	37.32
17	8.95	1.34	29.34
18	103.93	1.36	38.82
19	26.65	1.29	34.53
20	64.46	1.04	39.57
21	83.81	1.10	39.64
22	28.42	1.38	34.06
23	117.06	1.88	36.13
24	57.44	1.19	37.72
25	9.43	1.42	28.65

For cohesion (Figure 8a), the mean response curves identify the optimal factor levels as FL = 9 mm (Level 2), FC = 0.7% (Level 3), and WC = 6% (Level 2). Water content exhibits the most pronounced variation in mean cohesion, which peaks at 89.27 kPa under 6% WC and drops to 9.55 kPa under 12.5% WC (Level 5). For the internal friction angle (Figure 9a), the overall fluctuation range of φ is far narrower than that of c, indicating that the internal friction angle is much less sensitive to fiber parameters.

Range analysis results (Figures 8b and 9b) consistently identify water content as the dominant influencing factor for both shear strength parameters. The range R values of WC are 79.72 kPa for c and 14.74° for φ, far exceeding those of FC (21.63 kPa, 3.03°) and FL (11.46 kPa, 1.89°). This confirms that water content exerts a far stronger control on the shear strength of PP-GS than fiber parameters, while fiber length has the weakest effect. Frequency distribution histograms (Figures 8c and 9c) show that both c and φ follow left-skewed distributions, with their median values (57.26 kPa for c, 37.32° for φ) higher than their mean values (52.39 kPa, 36.04°). This distribution pattern is consistent with the design of orthogonal tests covering both optimal and inferior parameter combinations, and the reasonable data dispersion provides a reliable basis for subsequent parameter optimization and empirical model fitting.

ANOVA results (Figures 8d,e and 9d,e) further quantify the statistical significance of each factor. For cohesion, all three factors reach statistical significance: WC has an extremely significant effect ($p < 0.001$), FC also shows extremely significant influence ($p = 0.002 < 0.01$), and FL exerts a significant effect ($p = 0.013 < 0.05$). For the internal friction angle, by contrast, only WC exhibits an extremely significant effect ($p < 0.001$), while both FL ($p = 0.252$) and FC ($p = 0.124$) fail to reach statistical significance. The Taguchi S/N ratio response curves (Figures 8f and 9f) are in excellent agreement with the mean response

results, confirming the reliability of the identified optimal parameter combinations and further verifying the dominant role of water content.

Consistent with the unconfined compressive strength and peak shear strength results presented in Sections 4.1 and 4.2, the optimal fiber combination for maximizing cohesion is 9 mm FL and 0.7% FC. This configuration yields the highest reinforcement coefficient *K* (2.22 at 10.5% WC and 1.88 at 4% WC, as shown in Table 7), which is significantly higher than those of other fiber schemes, confirming a synergistic enhancement effect on the shear resistance of PP-GS.

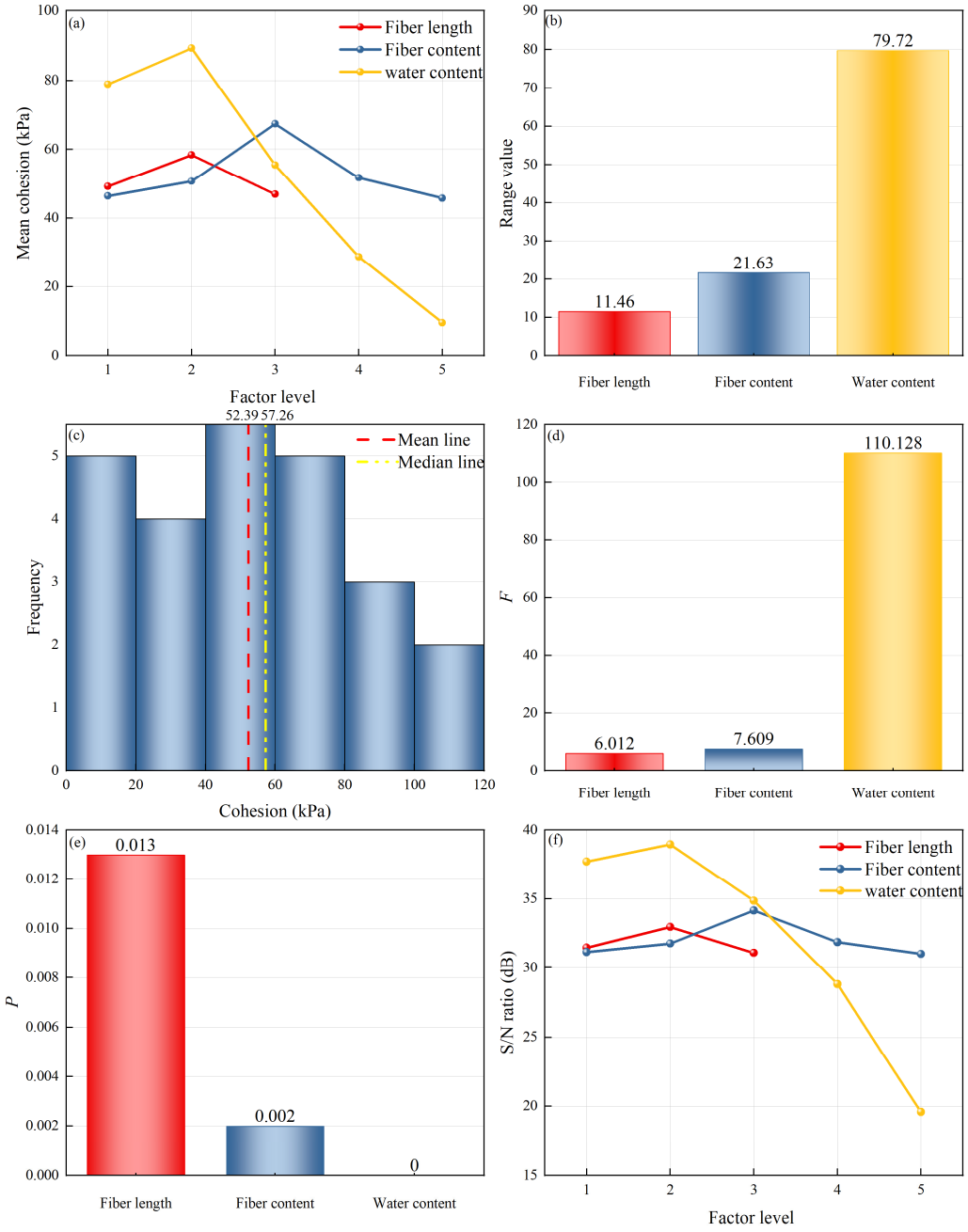


Figure 8. Multi-dimensional analysis of cohesion for PP-GSs in orthogonal direct shear tests: (**a**) mean response of cohesion to factor levels; (**b**) range values for cohesion factors; (**c**) frequency distribution of cohesion; (**d**) ANOVA F-values for cohesion factors; (**e**) ANOVA *p*-values for cohesion factors; (**f**) S/N ratio response of cohesion.

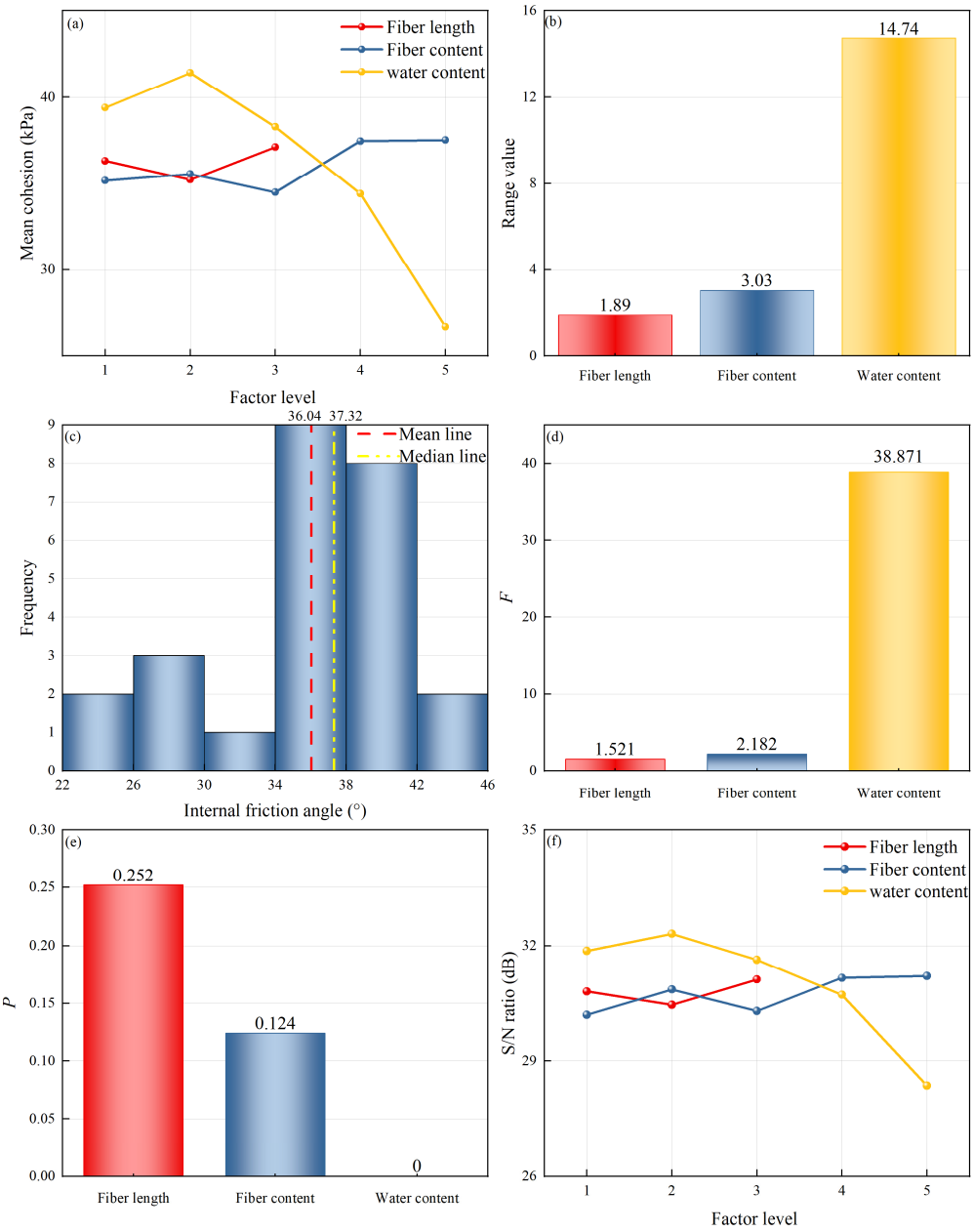


Figure 9. Multi-dimensional analysis of internal friction angle for PP-GS in orthogonal direct shear tests: (**a**) mean response of internal friction angle to factor levels; (**b**) range values for internal friction angle factors; (**c**) frequency distribution of internal friction angle; (**d**) ANOVA F-values for internal friction angle factors; (**e**) ANOVA *p*-values for internal friction angle factors; (**f**) S/N ratio response of internal friction angle.

4.2.3. Empirical Models for Shear Strength

Establishing empirical correlations between mechanical parameters and key controlling variables holds considerable practical significance for geotechnical engineering design and construction [69]. As demonstrated in the preceding statistical analyses, the shear strength parameters of PP-reinforced Gobi soil (PP-GS) are primarily governed by three independent variables: fiber length, fiber content, and initial water content. Accordingly, nonlinear curve fitting was conducted using Origin software (2024b) to characterize the quantitative relationships between the shear strength parameters and these three influencing factors. The derived fitting equations are summarized in Table 8. All equations produce coefficients of determination (R^2) above 0.88, indicating that the proposed nonlinear corre-

lations can satisfactorily describe the variation patterns of shear strength parameters within the tested variable ranges. Nevertheless, these empirical formulas are developed based on a limited set of laboratory test data; their broader generalizability and field engineering applicability still require further validation through extended systematic experiments and practical engineering applications.

Table 8. Nonlinear Fitting Results of Shear Strength Parameters.

Shear Strength Indices	Fitting Parameter					R^2	Fitting Formulation
Cohesion c	a_0 22.59	a_1 11.59	a_2 103.39	a_3 −0.31	a_{11} −0.92	0.90	$f = a_0 + a_1x + a_2y + a_3z + a_{11}x^2 + a_{22}y^2 + a_{33}z^2 + a_{12}xy + a_{13}xz + a_{23}yz$ x: Fiber length (mm) y: Fiber content (%) z: Water content (%)
	a_{22} −95.47	a_{33} −0.69	a_{12} 3.51	a_{13} 0.27	a_{23} 0.04		
Internal friction angle φ	a_0 26.55	a_1 −0.18	a_2 −0.35	a_3 4.24	a_{11} 0.03	0.88	
	a_{22} 3.05	a_{33} −0.35	a_{12} −0.22	a_{13} −0.01	a_{23} 0.19		

4.3. Disintegration Behavior

Soil disintegration is defined as the process whereby individual soil particles detach from the soil matrix under water immersion conditions [70]. According to the morphological features of disintegration curves, Liu et al. categorized soil disintegration into two distinct modes: complete disintegration and incomplete disintegration [71], as displayed in Figure 10a. The inclusion of polypropylene fibers converts the failure behavior of soil specimens from fast, full complete disintegration to slow, steady incomplete disintegration, demonstrating that fiber reinforcement effectively restrains soil disintegration. This observation is consistent with findings published in prior literature [72,73]. Disintegration curves for PP fiber-reinforced Gobi soil (PP-GS) are provided in Figure 10b. Unreinforced Gobi soil possesses prominent water sensitivity, and its disintegration ratio is strongly governed by initial water content: the total collapse durations for plain soil samples at water contents of 6%, 10.5%, and 12.5% are 2.3 min, 40 min, and 130 min, respectively. This reveals that elevated water content can retard disintegration progression yet cannot stop full disintegration in the end. Incorporating polypropylene fibers fundamentally modifies the disintegration pattern, transitioning the behavior from complete to incomplete disintegration per the classification of Liu et al. [71]. Under the optimal fiber parameters (9 mm length, 0.7% dosage), samples prepared at the three tested water contents all reach a stable disintegration plateau after roughly 240 min, though their final disintegration extents vary markedly. After 12 h of continuous immersion, the disintegration ratios measure 35%, 13%, and 3% for specimens with water contents of 6%, 10.5%, and 12.5%, respectively. Fiber length also acts as a vital factor controlling anti-disintegration performance. With fiber content fixed at the optimal 0.7% and water content maintained at 10.5%, samples reinforced with 6 mm, 9 mm, and 12 mm fibers yield 12 h disintegration ratios of 47%, 13%, and 15% respectively. This confirms an optimal fiber length of 9 mm within the scope of this experiment, which delivers a substantial improvement in the disintegration resistance of reinforced Gobi soil.

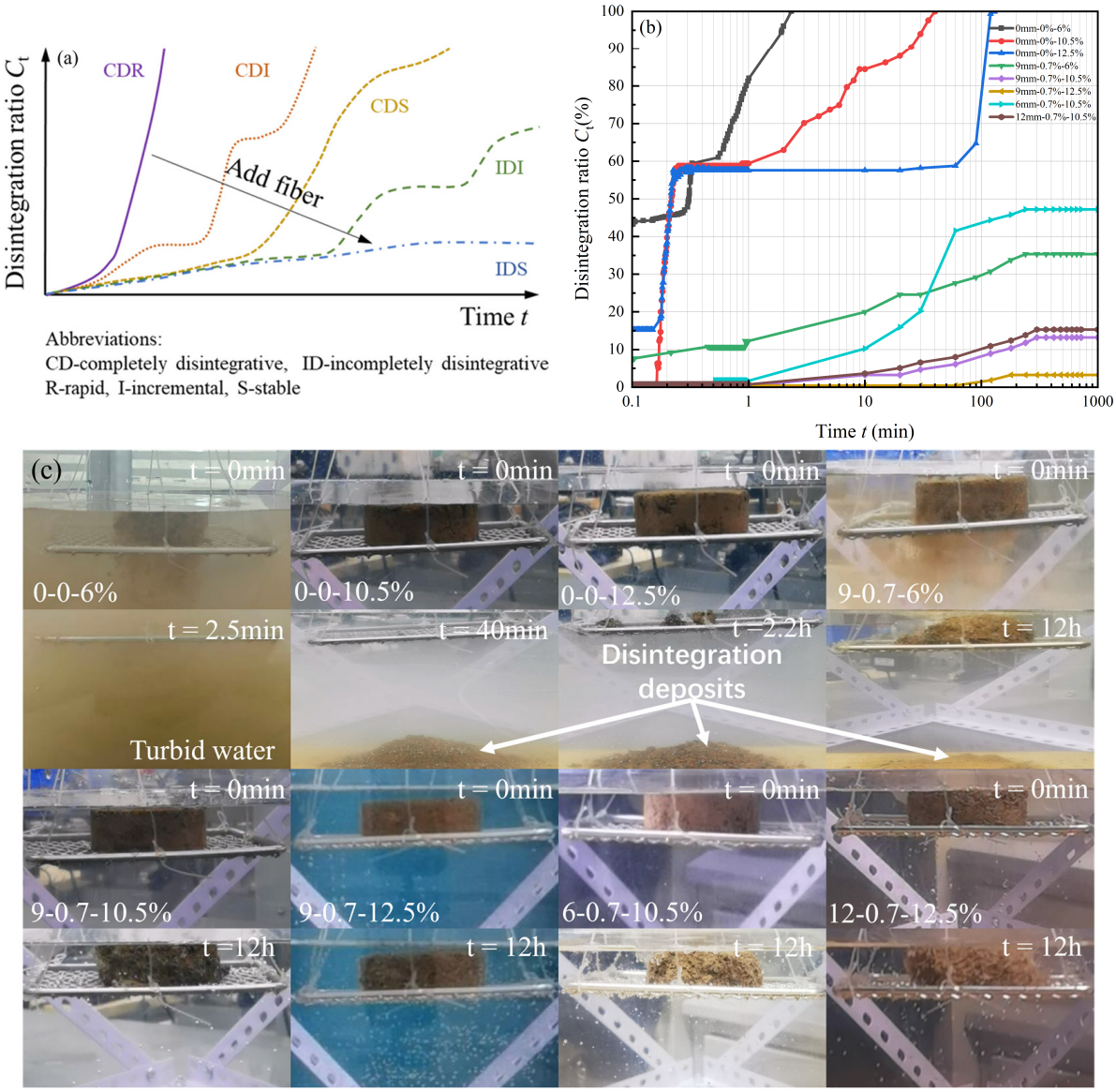


Figure 10. Water stability tests results of PP-GSs with different fiber lengths and water contents: (**a**) classification of disintegration [74]; (**b**) disintegration curves; (**c**) disintegration photographs.

The fundamental mechanisms triggering soil disintegration consist of two key factors: the dissolution of interparticle cementing bonds once soil contacts water, and swelling pressure generated by rapid water infiltration [75]. Unreinforced soil specimens collapse rapidly after submersion, as the breakdown of cementation eventually brings about complete disintegration. Polypropylene fibers improve the structural integrity of PP-GS by reinforcing interparticle contacts; even if partial cementation bonds are damaged by water intrusion, fibers remain capable of binding soil particles together. In addition, fibers withstand swelling pressure from infiltrating water, restrain crack expansion, and accordingly retard the disintegration rate [72]. Disintegration performance is highly dependent on fiber length: both excessively short and overly long fibers raise the disintegration ratio of PP-GS, with short fibers imposing a notably more adverse impact. In general, fiber inclusion boosts the water stability and submerged erosion resistance of reinforced Gobi soil, and a fiber length of 9 mm proves optimal in this test work. A higher initial water content (especially values close to the optimum water content) lowers suction gradients and uneven swelling stresses during immersion. This allows the three-dimensional fiber net-

work to constrain soil particles more effectively and suppress crack initiation and growth, substantially elevating overall water stability. Relying on their tensile capacity, fibers reinforce interparticle bonding; partial degradation of cementation still leaves fibers able to cluster particles and counteract swelling pressure from fast water penetration, restricting crack development [72]. Ultra-short 6 mm fibers cannot bridge multiple soil particles or microcracks to form a continuous reinforcing framework, yielding weak structural integrity and allowing water to easily permeate vulnerable zones. In contrast, overly long 12 mm fibers tend to bend, intertwine, and agglomerate locally during static compaction. This causes poor uniform dispersion, forms preferential seepage channels for fast water flow, and introduces localized weak planes within the soil matrix [72,73]. Fibers at the optimal length strike an ideal balance between continuous network formation and homogeneous dispersion, maximizing the mitigation and suppression of soil disintegration.

4.4. SEM Analysis

Figure 11 presents the SEM micrographs of PP-GS samples with various fiber contents at the optimal fiber length of 9 mm. For the unreinforced sample (0PP-GS, Figure 11a), scattered pores and microcracks exist throughout the soil matrix; these defects serve as stress concentration sites under load and induce brittle failure.

At fiber contents of 0.3% and 0.5% (Figure 11b,c), fibers build separate reinforcing junctions and boost stress transmission via mechanical interlocking. An incipient three-dimensional fiber network forms, yet the reinforcement performance remains restricted owing to inadequate fiber content. At the optimal fiber content of 0.7% (Figure 11d), fibers distribute evenly and randomly to construct a continuous three-dimensional network framework. Sufficient mechanical interlocking forms at fiber–soil particle interfaces, which efficiently restrains particle movement and inhibits crack growth.

When fiber content rises further to 0.9% and 1.1% (Figure 11e,f), fiber–fiber contact rises sharply, causing fiber agglomeration, overlapping and intertwining. This prevents adequate interfacial contact between fibers and soil particles and generates internal weak zones. Fiber clumps bridge neighboring micropores to create large interconnected voids and lower soil compactness. Such microstructural evolutions directly account for the macroscopic strength decline seen at excessively high fiber contents [76].

4.5. PP-GS Reinforcement Mechanism

Based on the experimental analysis and discussion above, polypropylene (PP) fibers can significantly improve the mechanical strength and water stability of Gobi soil (GS); however, the optimal reinforcement effect is achieved only when the fiber content is at an appropriate level. The macroscopic mechanical behavior and microstructural changes of the soil indicate that fiber incorporation exerts positive effects, mainly manifested as physical bonding between fibers and soil particles, fiber bridging, suppression of microcrack propagation, and confinement and reinforcement of soil particles by the three-dimensional network. The mechanical interlocking between PP fibers and Gobi soil particles forms a fiber–soil interfacial mechanical linkage structure (Figure 12a). This interface is dominated by physical interactions. The interlocking effect and interfacial frictional resistance enhance the occlusal constraint and load-transfer mechanism among soil particles, effectively inhibiting the sliding, dislocation, and discrete instability of coarse Gobi soil particles, thereby improving the structural integrity and mechanical stability of the soil. At the macroscopic level, this interfacial action not only significantly increases the compressive and shear strengths of Gobi soil and improves its crack resistance and deformation behavior but also enhances its durability against wind and water erosion.

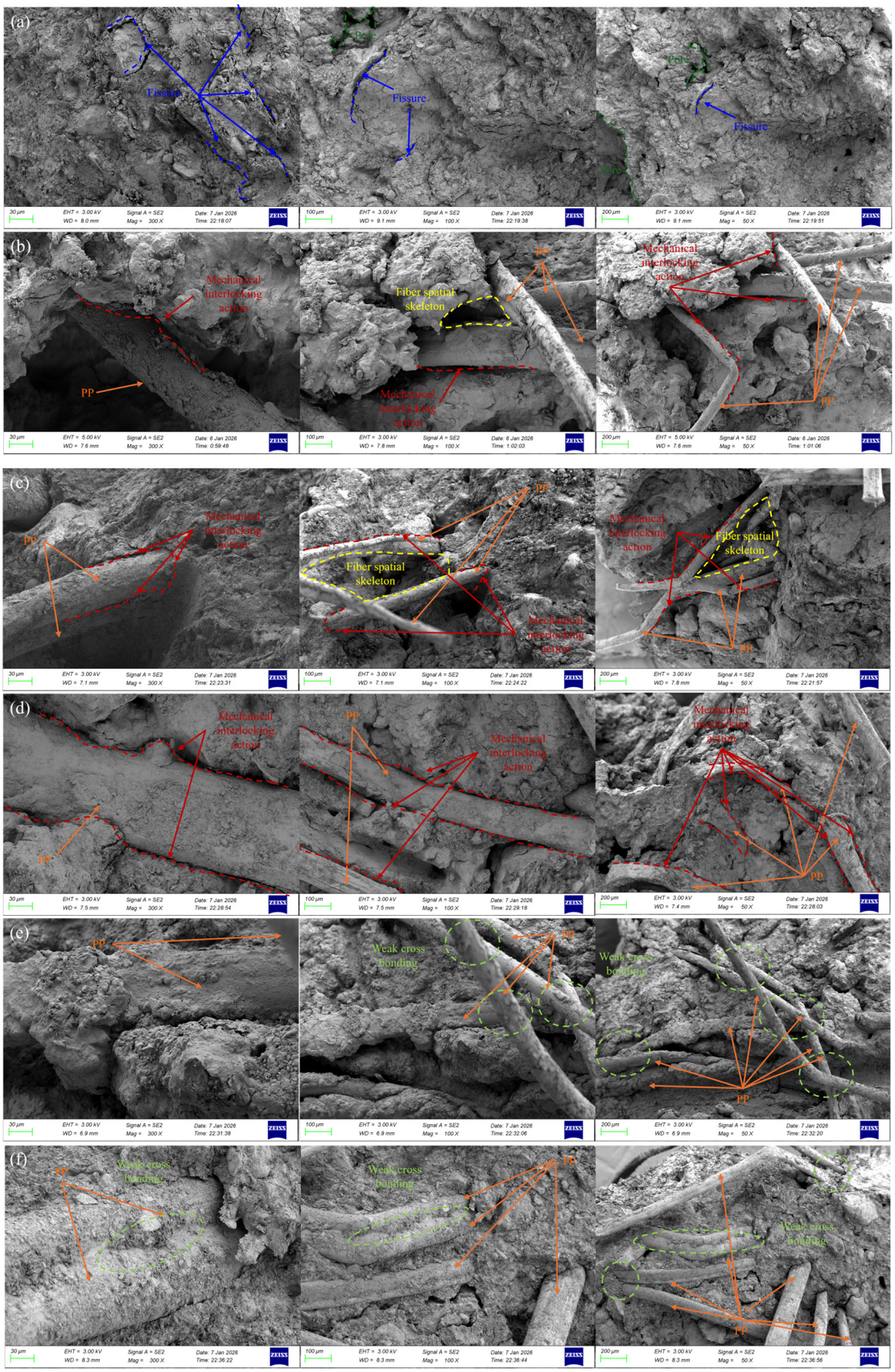


Figure 11. SEM Images for PP-GSs with different fiber contents: (**a**) for 0PP-GS; (**b**) for 0.3PP-GS; (**c**) for 0.5PP-GS; (**d**) for 0.7 PP-GS; (**e**) for 0.9 PP-GS; (**f**) for 1.1PP-GS.

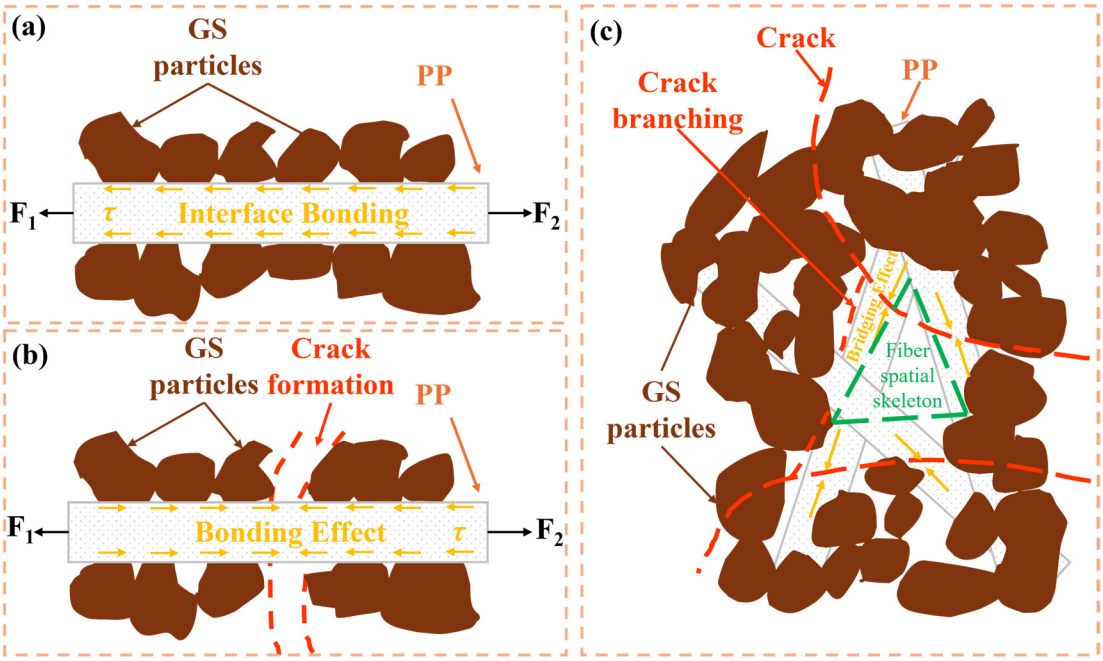


Figure 12. Schematic of mechanism of PP-GS: (**a**) interfacial bonding; (**b**) bridging effect; (**c**) cracks and fiber spatial skeleton.

When cracking occurs in the soil, the bridging effect of fibers suppresses crack propagation and reduces stress concentration (Figure 12b). Fiber breakage or pull-out consumes more external work. Consequently, even when cracks or large deformations appear, the fiber-reinforced soil can still sustain external loads, thus improving soil toughness. Under external loading, numerous microcracks initiate within the soil. When these microcracks propagate to a fiber, they tend to deflect or branch due to the obstruction by the fiber (Figure 12c). The restraining effect of fibers prolongs the effective crack propagation path, absorbing more external energy, and thereby enhances the mechanical strength and toughness of the soil. In addition, PP fibers are randomly distributed in three dimensions within the Gobi soil matrix, intertwining and overlapping to form a spatially continuous reinforcement network (also illustrated in Figure 12c). This network wraps, anchors, and omnidirectionally constrains soil particles, suppressing particle sliding, dislocation, and loosening. Simultaneously, the fiber network enables uniform transfer and diffusion of localized stress concentrations, synergistically utilizing the tensile strength of fibers and the shear strength of the soil. Thus, the network improves the structural integrity, mechanical stability, deformation resistance, and bearing capacity of Gobi soil at a three-dimensional scale.

Fiber-reinforced soil is widely used in geotechnical engineering, including slope engineering, foundation engineering, and subgrade engineering [76]. Polypropylene (PP) fiber, owing to its excellent engineering performance in reinforcing Gobi soil (GS), can serve as an effective material for soil reinforcement. The addition of PP fiber improves the mechanical properties and water stability of Gobi soil, thereby enhancing its bearing capacity. In the earthquake-prone Xinjiang region, the high toughness of PP-GS composite material helps improve the seismic performance of buildings; meanwhile, its low disintegration characteristic further increases the soil's erosion resistance. Furthermore, the application of PP-GS composite material promotes the resource utilization of waste polypropylene. This environmentally friendly and low-carbon soil improvement technology contributes to the sustainable development of both the economy and the environment.

5. Conclusions

This study systematically investigates the improvement effects of polypropylene fiber on the mechanical properties and water stability of Gobi soil through experimental tests. The main conclusions are as follows:

(1) Polypropylene fiber reinforcement significantly improves the mechanical behavior of Gobi soil, transforming the failure mode from brittle to ductile. The optimal fiber length and content are identified as 9 mm and 0.7%, respectively, achieving the most substantial strength enhancement.

(2) Water content dominates the shear strength indices of Gobi soil, with a far greater influence than fiber parameters. The optimal fiber combination (9 mm, 0.7%) yields a cohesion reinforcement coefficient of 2.22 at the construction-recommended Proctor optimum moisture content of 10.5%. Fiber parameters show no significant effect on the internal friction angle.

(3) Polypropylene fibers notably enhance the short-term water stability of Gobi soil, fundamentally changing the disintegration mode from complete rapid disintegration to incomplete stable disintegration. Under the optimal fiber parameters, the 12 h disintegration ratio is reduced from 100% to 13% at a water content of 10.5%, effectively inhibiting water-induced erosion.

(4) Microscopic observation shows that an appropriate fiber content forms a uniform three-dimensional network within the soil matrix, enhancing interparticle mechanical interaction. Excessive fiber content induces agglomeration and pore connectivity, compromising soil integrity.

The proposed PP fiber reinforcement method offers a low-carbon, sustainable approach for stabilizing Gobi soil in photovoltaic power station foundations. This study has limitations, including a limited number of parallel specimens, the size effect of direct shear specimens, the use of cited plain soil baseline data, and a lack of long-term environmental cycle tests and quantitative life cycle assessment. Further work will optimize test schemes and verify the long-term engineering performance and low-carbon benefits of this method.

Author Contributions: J.W. (Jiayu Wang): Writing—original draft, Formal analysis, Data curation; X.L.: Methodology, Writing—review & editing, Funding acquisition; Z.Z.: Investigation, Validation; J.W. (Jin Wu): Supervision, Formal analysis; D.W.: Writing—review & editing, Conceptualization. All authors have read and agreed to the published version of the manuscript.

Funding: This research was funded by The Third Batch Xinjiang Tianchi Doctoral Project (Grant No. 5105250182b).

Data Availability Statement: Data available upon request from the authors.

Acknowledgments: The authors would like to express sincere thanks to the editor and anonymous reviewers for their constructive and professional comments and suggestions regarding this manuscript.

Conflicts of Interest: The authors declare no conflicts of interest.

References

1. Hashemizadeh, A.; Abadi, F.Z.B.; Fan, C. Geopolitical perspective on global renewable energy development considering China's technological and Belt & Road scenarios. *Renew. Energy* **2026**, *256*, 124106. [CrossRef]
2. Hua, Y.T.; Tong, T.J. Renewable energy integration in the Belt and Road Initiative: Government expenditure, green finance, and economic growth. *Renew. Energy* **2026**, *256*, 123980. [CrossRef]
3. Hou, Z.M.; Xiong, Y.; Luo, J.S.; Fang, Y.L.; Haris, M.; Chen, Q.J.; Yue, Y.; Wu, L.; Wang, Q.C.; Huang, L.C. International experience of carbon neutrality and prospects of key technologies: Lessons for China. *Pet. Sci.* **2023**, *20*, 893–909. [CrossRef]

4. Wu, J.W.; Xiao, J.Y.; Hou, J.M.; Lyu, X. Development Potential Assessment for Wind and Photovoltaic Power Energy Resources in the Main Desert-Gobi-Wilderness Areas of China. *Energies* **2023**, *16*, 4559. [CrossRef]
5. Enebish, N. Developing Very Large Scale Solar Power plants in the Gobi desert to contribute for North East Asia's energy transition. In Proceedings of the 2025 IEEE 53rd Photovoltaic Specialists Conference (PVSC), Montreal, QC, Canada, 8–13 June 2025; pp. 0842–0844.
6. Harichandan, S.; Kar, S.K.; Bansal, R.; Mishra, S.K.; Balathanigaimani, M.S.; Dash, M. Energy transition research: A bibliometric mapping of current findings and direction for future research. *Clean. Prod. Lett.* **2022**, *3*, 100026. [CrossRef]
7. Si, L.J.; Wang, P.Y.; Cao, D.Q. Towards sustainable development goals: Assessment of wind and solar potential in northwest China. *Environ. Res.* **2024**, *252*, 118660. [CrossRef] [PubMed]
8. Li, L.; Wang, X.Y.; Luo, L.; Zhao, Y.C.; Zong, X.; Bachagha, N. Mapping of wind energy potential over the Gobi Desert in Northwest China based on multiple sources of data. *Front. Earth Sci.* **2018**, *12*, 264–279. [CrossRef]
9. Zhao, W.J.; Zhao, J.; Liu, M.Y.; Gao, Y.; Li, W.L.; Duan, H.W. Vegetation Restoration Increases Soil Carbon Storage in Land Disturbed by a Photovoltaic Power Station in Semi-Arid Regions of Northern China. *Agronomy* **2024**, *14*, 9. [CrossRef] [PubMed]
10. Elsonbaty, L.; Fawzy, H.E.; Moghazy, H.M.; Rashed, G.; Hamed, M. Vertical accuracy assessment for open-source digital elevation models using GPS control points and watershed basins delineation using GIS. *Alex. Eng. J.* **2023**, *84*, 47–58. [CrossRef]
11. Marin-Lopez, C.; Lopez-Lara, T.; Hernandez-Zaragoza, J.; Horta-Rangel, J.; Rojas-Gonzalez, E.; Perez-Rea, M.; Salgado-Delgado, R.; Salgado-Delgado, A.; Castano, V. The effect of the grain-size distribution on expansion and collapse behavior of expansive soils and their implications. *Int. J. Geosynth. Ground Eng.* **2022**, *8*, 10. [CrossRef]
12. de Albuquerque, P.J.R.; Carvalho, D.d.; Kassouf, R.; Fonte, N.L., Jr. Behavior of laterally top-loaded deep foundations in highly porous and collapsible soil. *J. Mater. Civ. Eng.* **2019**, *31*, 04018373. [CrossRef]
13. Kassouf, R.; Carvalho, D.d.; Albuquerque, P.J.R.-d. The behavior of a foundation transversally loaded at the top over highly porous and collapsible soil. *Dyna* **2016**, *83*, 134–139. [CrossRef]
14. Kalantari, B. Foundations on collapsible soils: A review. *Proc. Inst. Civ. Eng.-Forensic Eng.* **2013**, *166*, 57–63. [CrossRef]
15. Lian, J.J.; Zhao, Y.Q.; Li, J.L.; Guo, Y.H.; Wang, H.J. Vertical bearing behavior and influence depth of the five-bucket foundation for offshore wind turbines in layered soil conditions. *Ocean Eng.* **2025**, *342*, 122997. [CrossRef]
16. Ding, H.Y.; Peng, Y.J.; Zhang, P.Y.; Nie, L.Y.; Zhai, H.B. Numerical Simulation of Vacuum Preloading for Reinforcing Soil inside Composite Bucket Foundation for Offshore Wind Turbines. *J. Mar. Sci. Eng.* **2019**, *7*, 273. [CrossRef]
17. Piccinelli, S.; Brusa, G.; Cannone, N. Climate warming accelerates forest encroachment triggered by land use change: A case study in the Italian Prealps (Triangolo Lariano, Italy). *CATENA* **2020**, *195*, 104870. [CrossRef]
18. Xu, K.M.; Jiang, G.L.; Chen, J.; Wu, Q.B. Thermal stability of permafrost under U-shaped crushed rock embankment of the Qinghai-Tibet Railway. *Adv. Clim. Change Res.* **2024**, *15*, 158–169. [CrossRef]
19. Guo, Q.; Amin, S.; Wang, H.; Yan, H. Coupling Simulation of Human-Environmental Safety Risk Factors in Metro Construction—A Case Study of Rongjiazhai Station at Xi'an Metro Line 5 in China. *Int. J. Constr. Educ. Res.* **2023**, *20*, 26–42. [CrossRef]
20. Hu, X.R.; Fu, X.L.; Peng, M.; Zhang, G.D.; Shi, Z.M.; Zhu, Y.; Li, Y.C. Experimental and numerical study on the breaching mechanisms of landslide dams with non-uniform structures. *Eng. Geol.* **2024**, *330*, 107414. [CrossRef]
21. Bui, D.T.; Moayedi, H.; Gör, M.; Jaafari, A.; Foong, L.K. Predicting Slope Stability Failure through Machine Learning Paradigms. *Isprs Int. J. Geo-Inf.* **2019**, *8*, 395. [CrossRef]
22. Che, F.; Yin, C.; Zhang, H.; Tang, G.T.; Hu, Z.N.; Liu, D.; Li, Y.; Huang, Z.F. Assessing the Risk Probability of the Embankment Seismic Damage Using Monte Carlo Method. *Adv. Civ. Eng.* **2020**, *2020*, 8839400. [CrossRef]
23. Lee, J.K.; Jung, Y.H. Evaluation of Surface Ground Vibrations Induced by Tunnel Blasts During Railway Construction: A Case Study. *Transp. Infrastruct. Geotechnol.* **2024**, *11*, 2885–2902. [CrossRef]
24. Manny, L.; Angst, M.; Rieckermann, J.; Fischer, M. Socio-technical networks of infrastructure management: Network concepts and motifs for studying digitalization, decentralization, and integrated management. *J. Environ. Manag.* **2022**, *318*, 115596. [CrossRef] [PubMed]
25. Lin, P.; Yuan, X.-X. Performance of reliability-based design formats in geotechnical applications. *Rock Mech. Bull.* **2023**, *2*, 100025. [CrossRef]
26. Wang, C. A generalized index for functionality-sensitive resilience quantification. *Resilient Cities Struct.* **2023**, *2*, 68–75. [CrossRef]
27. Yusuf, M.; Agbahiwe, O.K.; Animashaun, T.A.; Borokinni, M.; Alabi, R.O.; Olayode, A. Advances in Sustainable Geotechnical Engineering: A Review of Bio-mediated Soil Stabilisation, Cellular Confinement Systems, and Waste-Based Soil Improvements. *Path Sci.* **2025**, *11*, 7009–7021. [CrossRef]
28. Vincevica-Gaile, Z.; Teppand, T.; Kriipsalu, M.; Krievans, M.; Jani, Y.; Klavins, M.; Setyobudi, R.H.; Grinfelde, I.; Rudovica, V.; Tamm, T.; et al. Towards Sustainable Soil Stabilization in Peatlands: Secondary Raw Materials as an Alternative. *Sustainability* **2021**, *13*, 6726. [CrossRef]
29. Xu, Y.; Wang, L.Y.; Li, K.K.; Wei, L.Y.; Chen, C.; Xiang, L.J.; Cai, J.X.; Wang, Z. Multi-tier life cycle assessment for evaluating low carbon strategies in soil remediation. *Environ. Impact Assess. Rev.* **2024**, *106*, 107491. [CrossRef]

30. Chen, X.; Xu, D.W.; Fadelelseed, S.; Li, L.Y. Spatiotemporal Analysis and Control of Landscape Eco-Security at the Urban Fringe in Shrinking Resource Cities: A Case Study in Daqing, China. *Int. J. Environ. Res. Public Health* **2019**, *16*, 4640. [CrossRef] [PubMed]
31. Barwar, A.; Chandrappa, A.K.; Sahoo, U.C. Laboratory investigations on stabilization of weak clay soil using rice husk ash and cement. *Innov. Infrastruct. Solut.* **2022**, *7*, 327. [CrossRef]
32. Li, T.; Yang, H.L.; Xu, L.T.; Zhou, Y.T.; Min, Y.J.; Yan, S.C.; Zhang, Y.H.; Wang, X.M. Comprehensive treatment strategy for diesel truck exhaust. *Environ. Sci. Pollut. Res.* **2023**, *30*, 54324–54332. [CrossRef] [PubMed]
33. Ping, L.; Zhao, G.; Lin, X.H.; Gu, Y.H.; Liu, W.; Cao, H.H.; Huang, J.W.; Xu, J.C. Feasibility and Carbon Footprint Analysis of Lime-Dried Sludge for Cement Production. *Sustainability* **2020**, *12*, 2500. [CrossRef]
34. Roche, M.Y. Built for net-zero: Analysis of long-term greenhouse gas emission pathways for the Nigerian cement sector. *J. Clean. Prod.* **2023**, *383*, 135446. [CrossRef]
35. Satola, D.; Balouktsi, M.; Lützkendorf, T.; Wiberg, A.H.; Gustavsen, A. How to define (net) zero greenhouse gas emissions buildings: The results of an international survey as part of IEA EBC annex 72. *Build. Environ.* **2021**, *192*, 107619. [CrossRef]
36. Chang, Q.Y.; Liu, L.L.; Farooqi, M.U.; Thomas, B.; Özkilic, Y.O. Data-driven based estimation of waste-derived ceramic concrete from experimental results with its environmental assessment. *J. Mater. Res. Technol.* **2023**, *24*, 6348–6368. [CrossRef]
37. Nanda, R.P.; Priya, N. Geopolymer as stabilising materials in pavement constructions: A review. *Clean. Waste Syst.* **2024**, *7*, 100134. [CrossRef]
38. Li, Z.N.; Zhang, F.M.; Gu, W.; Dong, M.L. The Niushou landslide in Nanjing City, Jiangsu Province of China: A slow-moving landslide triggered by rainfall. *Landslides* **2020**, *17*, 2603–2617. [CrossRef]
39. Jalali, J.; Noorzad, R. Discrete fiber reinforcement efficiency in the mechanical properties and wet-dry performance of fat clay treated with industrial sewage sludge ash. *Constr. Build. Mater.* **2021**, *284*, 122739. [CrossRef]
40. Soleimani-Fard, H.; König, D.; Goudarzy, M. Plane strain shear strength of unsaturated fiber-reinforced fine-grained soils. *ACTA Geotech.* **2022**, *17*, 105–118. [CrossRef]
41. Kar, R.; Pradhan, P. Strength and compressibility characteristics of randomly distributed fiber-reinforced soil. *Int. J. Geotech. Eng.* **2011**, *5*, 235–243. [CrossRef]
42. Evangelou, E.D.; Markou, I.N.; Verykaki, S.E.; Bantralexis, K.E. Mechanical behavior of fiber-reinforced soils under undrained triaxial loading conditions. *Geotechnics* **2023**, *3*, 874–893. [CrossRef]
43. Mardani, A.; Hataf, N. Experimental investigation into the mechanical behavior of fine-grained soils reinforced with a newly developed branched fiber: A comparative study. *Arab. J. Geosci.* **2024**, *17*, 51. [CrossRef]
44. Li, L.H.; Zang, T.B.; Xiao, H.L.; Feng, W.Q.; Liu, Y.L. Experimental study of polypropylene fibre-reinforced clay soil mixed with municipal solid waste incineration bottom ash. *Eur. J. Environ. Civ. Eng.* **2023**, *27*, 2700–2716. [CrossRef]
45. Wang, S.N.; Xue, Q.P.; Ma, W.; Zhao, K.; Wu, Z.J. Experimental study on mechanical properties of fiber-reinforced and geopolymer-stabilized clay soil. *Constr. Build. Mater.* **2021**, *272*, 121914. [CrossRef]
46. Xiao, Y.; Tong, L.Y.; Che, H.B.; Guo, Q.W.; Pan, H.S. Experimental studies on compressive and tensile strength of cement-stabilized soil reinforced with rice husks and polypropylene fibers. *Constr. Build. Mater.* **2022**, *344*, 128242. [CrossRef]
47. Lu, J.G.; Liu, J.N.; Yang, H.H.; Wan, X.S.; Gao, J.J.; Zhang, J.C.; Li, P.C. Experimental investigation on the mechanical properties and pore structure deterioration of fiber-reinforced concrete in different freeze-thaw media. *Constr. Build. Mater.* **2022**, *350*, 128887. [CrossRef]
48. Ahmadi, S.; Ghasemzadeh, H.; Changizi, F. Effects of A low-carbon emission additive on mechanical properties of fine-grained soil under freeze-thaw cycles. *J. Clean. Prod.* **2021**, *304*, 127157. [CrossRef]
49. Liu, C.; Lv, Y.R.; Yu, X.J.; Wu, X. Effects of freeze-thaw cycles on the unconfined compressive strength of straw fiber-reinforced soil. *Geotext. Geomembr.* **2020**, *48*, 581–590. [CrossRef]
50. Moslemi, A.; Tabarsa, A.; Mousavi, S.Y.; Monfared, M.H.A. Shear strength and microstructure characteristics of soil reinforced with lignocellulosic fibers-Sustainable materials for construction. *Constr. Build. Mater.* **2022**, *356*, 129246. [CrossRef]
51. Khorram, N.; Rajabi, A.M. Strength properties and microstructural characteristics of clay treated with alkali activated mortar and fiber. *Constr. Build. Mater.* **2022**, *341*, 127486. [CrossRef]
52. Owino, A.O.; Hossain, Z. The influence of basalt fiber filament length on shear strength development of chemically stabilized soils for ground improvement. *Constr. Build. Mater.* **2023**, *374*, 130930. [CrossRef]
53. Onochie, K.K.; Balkis, A.P. Polypropylene fiber reinforced Alker as a structurally stable and sustainable building material. *J. Clean. Prod.* **2021**, *279*, 123600. [CrossRef]
54. Shen, Y.S.; Tang, Y.; Yin, J.; Li, M.P.; Wen, T. An experimental investigation on strength characteristics of fiber-reinforced clayey soil treated with lime or cement. *Constr. Build. Mater.* **2021**, *294*, 123537. [CrossRef]
55. Sujatha, E.R.; Atchaya, P.; Darshan, S.; Subhashini, S. Mechanical properties of glass fibre reinforced soil and its application as subgrade reinforcement. *Road Mater. Pavement Des.* **2021**, *22*, 2384–2395. [CrossRef]
56. Mukherjee, K.; Mishra, A.K. Undrained performance of sustainable compacted sand- bentonite-glass fiber composite for landfill application. *J. Clean. Prod.* **2020**, *244*, 118662. [CrossRef]

57. Zaimoglu, A.S.; Yetimoglu, T. Strength behavior of fine grained soil reinforced with randomly distributed polypropylene fibers. *Geotech. Geol. Eng.* **2012**, *30*, 197–203.
58. Krishna, T.M.; Beebi, S.S. Soil stabilization by groundnut shell ash and waste fiber material. *Int. J. Innov. Eng. Technol.* **2015**, *5*, 52–57.
59. Develioglu, I.; Pulat, H.F. Shear strength of alluvial soils reinforced with PP fibers. *Bull. Eng. Geol. Environ.* **2021**, *80*, 9237–9248. [CrossRef]
60. Darvishi, A.; Vosoughifar, H.; Saeidijam, S.; Torabi, M.; Rahmani, A. An experimental and prediction study on the compaction and swell–expansion behavior of bentonite clay containing various percentages of two different synthetic fibers. *Innov. Infrastruct. Solut.* **2020**, *5*, 31. [CrossRef]
61. Phanikumar, B.R.; Singla, R. Swell-consolidation characteristics of fibre-reinforced expansive soils. *Soils Found.* **2016**, *56*, 138–143. [CrossRef]
62. Correia, N.; Rocha, S.; Lodi, P.; McCartney, J. Shear strength behavior of clayey soil reinforced with polypropylene fibers under drained and undrained conditions. *Geotext. Geomembr.* **2021**, *49*, 1419–1426. [CrossRef]
63. Falamaki, A.; Shafiee, A.; Eskandari, M.; Mohamadzadebabr, K. Choice of fiber-reinforced base material to reduce internal erosion mass transport. *Arab. J. Geosci.* **2020**, *13*, 236. [CrossRef]
64. de Albuquerque, P.J.R.; León-Mogrovejo, D.R. A laboratory investigation on a mechanical behavior of sandy and clayey soils with kraft paper fiber. *Transp. Infrastruct. Geotechnol.* **2021**, *8*, 12–36.
65. Chegenizadeh, A.; Nikraz, H. Synthetic Polypropylene Fiber Application in Soil. *Adv. Mater. Res.* **2012**, *550*, 827–833. [CrossRef]
66. Noorzad, R.; Zarinkolaei, S.T.G. Comparison of Mechanical Properties of Fiber-Reinforced Sand under Triaxial Compression and Direct Shear. *Open Geosci.* **2015**, *7*, 547–558. [CrossRef]
67. Liu, X.Y.; Wang, J.Y.; Wu, J. Influence of Compaction and Water Content on the Shear Performance of Gobi Soil as a Sustainable Construction Material. *Appl. Sci.* **2025**, *15*, 13089. [CrossRef]
68. *GB/T50123-2019*; Standard for Geotechnical Testing Method. China Planning Press: Beijing, China, 2019.
69. Zhang, Y.J.; Deng, P.Y.; Yang, Z.B.; Wang, Y. Statistical analysis of physical and mechanical parameters of soil-rock mixture in China. *Eng. Res. Express* **2025**, *7*, 045103. [CrossRef]
70. Zhang, X.W.; Kong, L.W.; Li, J.J. Influence of dry and wet seasons on disintegration characteristics of basalt residual soil from the Leizhou Peninsula, China. *Q. J. Eng. Geol. Hydrogeol.* **2018**, *51*, 450–460. [CrossRef]
71. Liu, X.Y.; Zhang, X.W.; Kong, L.W.; Wang, G.; Lu, J.F. Disintegration of granite residual soils with varying degrees of weathering. *Eng. Geol.* **2022**, *305*, 106723. [CrossRef]
72. An, N.; Yan, C.; Wang, Y.; Lan, H.; Bao, H.; Xu, J.; Shi, Y.; Sun, W. Experimental study on anti-erosion performance of polypropylene fiber-reinforced loess. *Rock Soil Mech.* **2021**, *42*, 501–510.
73. Bao, H.; Liu, C.Q.; Lan, H.X.; Yan, C.G.; Li, L.P.; Zheng, H.; Dong, Z.G. Time-dependency deterioration of polypropylene fiber reinforced soil and guar gum mixed soil in loess cut-slope protecting. *Eng. Geol.* **2022**, *311*, 106895. [CrossRef]
74. Wu, D.; Wang, C.M.; Liu, H.L.; Liu, X.Y.; Wang, H.L.; Wang, Q.Y. Recycled polyester fiber reinforcing red mud-improved volcanic ash as a sustainable construction material. *Constr. Build. Mater.* **2024**, *413*, 134821. [CrossRef]
75. Zhang, X.-W.; Kong, L.-W.; Zhang, M. Engineering geological characteristics of basalt residual soils in Leizhou Peninsula. *Chin. J. Geotech. Eng.* **2014**, *36*, 855–863.
76. Tran, K.Q.; Satomi, T.; Takahashi, H. Effect of waste cornsilk fiber reinforcement on mechanical properties of soft soils. *Transp. Geotech.* **2018**, *16*, 76–84. [CrossRef]

Disclaimer/Publisher's Note: The statements, opinions and data contained in all publications are solely those of the individual author(s) and contributor(s) and not of MDPI and/or the editor(s). MDPI and/or the editor(s) disclaim responsibility for any injury to people or property resulting from any ideas, methods, instructions or products referred to in the content.